Dalton Transactions

ROYAL SOCIETY OF CHEMISTRY

PAPER

View Article Online
View Journal | View Issue

Cite this: *Dalton Trans.*, 2020, **49**, 11577

Slow magnetic relaxation in cobalt N-heterocyclic carbene complexes†

Mohamed R. Saber, [a,b] Jacob A. Przyojski,[c] Zachary J. Tonzetich [c] and Kim R. Dunbar *[a]

Received 28th June 2020,
Accepted 29th July 2020

DOI: 10.1039/d0dt02286a

rsc.li/dalton

The combined experimental and theoretical investigation of the magnetic properties of the cobalt(II) NHC complexes (NHC = N-heterocyclic carbene); $[Co(CH_2SiMe_3)_2(IPr)]$ (**1**), $[CoCl_2(IMes)_2]$ (**2**) and $[Co(CH_3)_2(IMes)_2]$ (**3**) revealed a large easy plane anisotropy for **1** (D = +73.7 cm^{-1}) and a moderate easy axis anisotropy for **2** (D = −7.7 cm^{-1}) due to significant out-of-state spin–orbit coupling. Dynamic magnetic measurements revealed slow relaxation of the magnetization for **1** (U_{eff} = 22.5 K, τ_0 = 3 × 10^{-7} s, 1000 Oe) and for **2** (U_{eff} = 20.2 K, τ_0 = 1.73 × 10^{-8} s, 1500 Oe). The molecular origin of the slow relaxation phenomena was further supported by the retention of AC signal in 10% solutions in 2-MeTHF which reveals a second zero field AC signal in **1** at higher frequencies. Compound **3** was found to be an S = 1/2 system.

Introduction

Magnetic bistability in coordination compounds has garnered major interest over the past few decades with recent expansion to the study of organometallic compounds and mononuclear metal complexes.[1–4] In particular, the observation of slow relaxation of the magnetization in mononuclear transition metal complexes provides an excellent opportunity to gain a deeper understanding into the origins of the single molecule magnet phenomenon and the different possibilities for enhancement.[3,5–8] Efforts towards dictating orbital contributions to the magnetic ground state *via* careful structural control of the local geometry and ligand field strength has led to remarkable examples of mononuclear low-coordinate SMMs with very high energy barriers.[3] Recent reports have suggested the possibility of using the ligand contribution to the overall spin–orbit coupling of the metal complex to enhance the magnetic anisotropy.[5]

Cobalt mononuclear complexes are currently one of the major classes of mononuclear transition metal SMMs. Magnetic bistability has been observed in cobalt compounds with a wide variety of coordination environments including octahedral,[9,10] tetrahedral,[5] pseudo-tetrahedral,[11] square pyramidal,[12] trigonal planar,[6,13] trigonal pyramidal,[8] and trigonal prismatic[14,15] geometries. Magnetic bistability has also been reported for organometallic compounds based on lanthanides.[16–19]

Earlier, Tonzetich and coworkers reported the syntheses, structures and catalytic activities of a family of cobalt(II) NHC complexes with trigonal planar, $[Co(CH_2SiMe_3)_2(IPr)]$ (**1**), pseudo-tetrahedral, $[CoCl_2(IMes)_2]$ (**2**), and square planar, $[Co(CH_3)_2(IMes)_2]$ (**3**), coordination environments.[20] This series of compounds is well suited for exhibiting high magnetic anisotropy which is expected to lead to magnetic bistability. A few magnetic studies for NHC complexes have been previously reported[21–27] including the similar three-coordinate iron(II) NHC alkyl complexes,[22–25] and the linear mononuclear SMMs, $[Co(IMes)_2][BPh_4]$ and $[Ni(6\text{-}Mes)_2]^+$.[26,27]

Results and discussion

Compound **1** exhibits a distorted trigonal planar local geometry (Fig. 1a) with C_{NHC}–Co–C_{alkyl} and C_{alkyl}–Co–C_{alkyl} angles of 118.67(8)° and 122.66(16)°, respectively. The electronic structure of trigonally coordinated metal centers with C_{2v} symmetry has been previously studied in the LMX family (L = diketiminate, M^{II} = Fe, Co, Ni and X = Cl, THF, CH_3)[28] and found to demonstrate a d orbital order of d_{z^2}, d_{yz}, $d_{x^2-y^2}$, d_{xz}, d_{xy}.[28–30] The Mössbauer and EPR studies of $LFeCH_3$ revealed a high spin iron site with large D values ($D \sim -100$ cm^{-1}) as well as significant orbital contributions despite the non-degenerate nature expected for the crystal field states of the metal center in idealized C_{2v} symmetry. The unquenched orbital contri-

[a]Department of Chemistry, Texas A&M University, College Station, TX 77842-3012, USA. E-mail: dunbar@mail.chem.tamu.edu
[b]Chemistry Department, Faculty of Science, Fayoum University, Fayoum 63514, Egypt
[c]Department of Chemistry, University of Texas at San Antonio (UTSA), San Antonio, TX 78249, USA

†Electronic supplementary information (ESI) available: Experimental data. See DOI: 10.1039/d0dt02286a

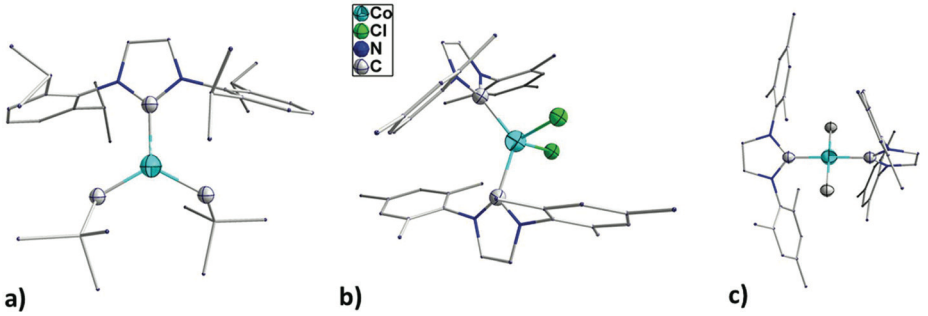

Fig. 1 Molecular structures of compounds **1** (a), **2** (b) and **3** (c). Phenyl rings were shown in wire model and hydrogen atoms were omitted for clarity. Images generated from crystallographic data in ref. 20.

bution is a result of orbital mixing in a nearly accidentally orbitally degenerate ground state (d_{z^2}, d_{yz}).[29] A similar electronic structure was reported for [Fe(7-DiPP)Br$_2$],[23,24] with the ZFS contributions being attributed to out-of-state spin–orbit coupling involving the 1 → 2 orbital excitation energy leading to a moderate D value (+16.8 cm^{-1}). Interestingly, the dihedral angle between the Br–Fe–Br and N–C–N planes has a significant effect on the relative energies of the ground state orbitals most likely due to the different alignment with the p-orbital on the carbene ligand. This shift in energy affects the 1 → 2 and 1 → 3 orbital excitations causing the 1 → 3 excitation to become more significant which leads to a change in the sign of D. The electronic structure of the isostructural Fe(II) analogue, [Fe(CH$_2$SiMe$_3$)$_2$(IPr)], was found to be $(d_{z^2})^2(d_{yz})^1(d_{xz})^1(d_{x^2-y^2})^1(d_{xy})^1$ which leads to a moderate negative D value of −19.9 cm^{-1}.[22,31] Computational studies of the electronic structure of the iron(I) compound, [LFe^{I}Cl]$^-$ (L = diketiminate), which possesses a d^7 configuration revealed moderate D values and quenched angular momentum due to the large separation of the excited states.[32] The introduction of a strong π-accepting ligand in LFe^{I}(HCCR) leads to a lower energy for the d_{xy} orbital which results in spin–orbit coupling of the two nearly degenerate $\{d_{z^2}\}$ and $\{d_{z^2} \rightarrow d_{yz}\}$ configurations, the consequence of which are large negative D values (−170 cm^{-1}).

With the previously reported results as a backdrop, magnetic measurements were performed on crushed single crystal samples of the compounds under a 1000 Oe field over the temperature range of 1.8–300 K. The χT value of [Co(CH$_2$SiMe$_3$)$_2$(IPr)] (**1**) at 300 K (3.15 emu mol^{-1} K) corresponds to one Co(II) center with significant orbital contributions (S = 3/2, g = 2.6). At lower temperatures, the χT value slowly decreases to a minimum of 1.98 emu mol^{-1} K at 2 K (Fig. 2). Both the high room temperature χT value and the slow decrease at lower temperatures for **1** are signatures of appreciable magnetic anisotropy. The lack of saturation in the magnetization *versus* field data up to 7 T (Fig. S1†) and the non-superimposable nature of the field-dependent magnetization data for **1** at temperatures between 1.8 and 4.5 K (Fig. S1†) support the anisotropic nature of the Co(II) center and indicate the presence of significant zero-field splitting. The χT and reduced

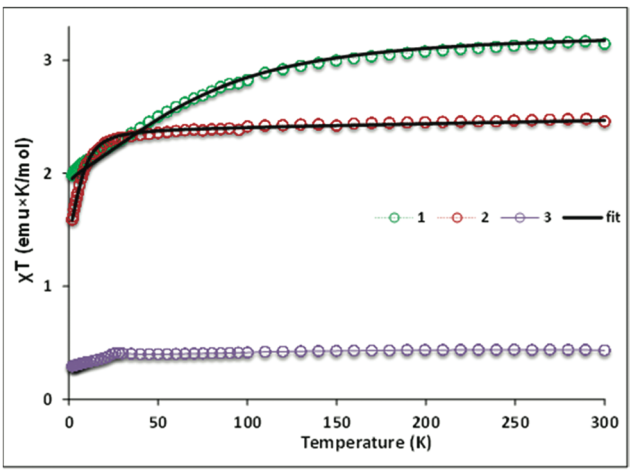

Fig. 2 Variable temperature DC magnetic susceptibility data for **1–3**. Solid lines represent fits using PHI (D = +73.7(±1), E = +19.2(±1) cm^{-1}, g = 2.63 for **1**, D = −7.7(±1), E = 1.2(±1) cm^{-1}, g = 2.29 for **2**).

magnetization data were simultaneously fitted with the PHI[33] program based on a spin 3/2 configuration using a zero-field splitting Hamiltonian. The results indicate a large positive D value with significant rhombicity (D = +73.7(±1) cm^{-1}, E = +19.2(±1) cm^{-1} and g = 2.63).

$$\hat{H} = D\left(\hat{S}_z^{\,2} - S(S+1)/3\right) + E\left(\hat{S}_x^{\,2} - \hat{S}_y^{\,2}\right) + g\mu_B \vec{B} \cdot \hat{S}. \quad (1)$$

Given the large D values observed for **1**, the possibility for slow relaxation of the magnetization was probed by dynamic magnetic studies in the absence of a field and under an applied field. The AC susceptibility measurements of **1** revealed no AC signals in the absence of an external static magnetic field. Upon applying a static DC field, a field induced out-of-phase AC signal up to 4.5 K was observed as depicted in Fig. 3. The optimum DC field was determined by varying the field for the frequency dependent AC measurements and found to be 1000 Oe (Fig. S2a†). The frequency dependent measurements in the range of ν (1–1500 Hz) were measured over the temperature range of 1.8–4.1 K under a 1000 Oe DC

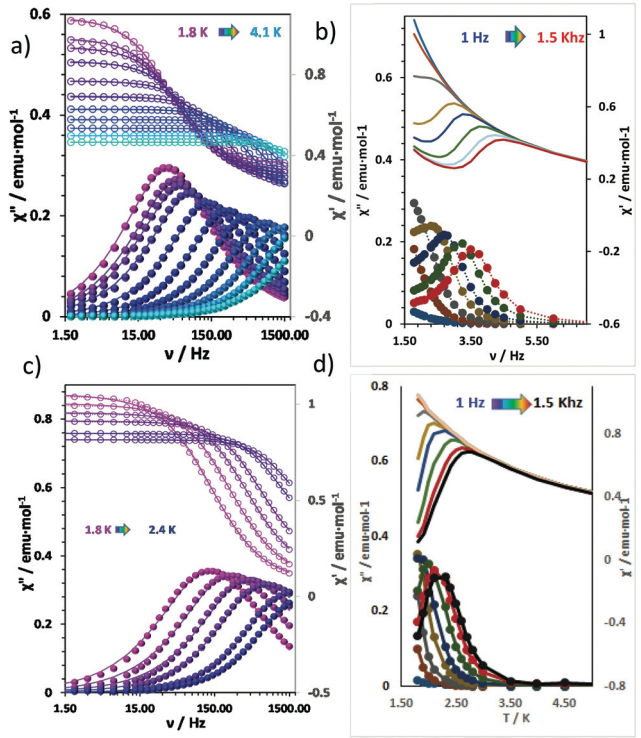

Fig. 3 Frequency (a) and temperature (b) dependence of the AC susceptibility data of **1** and **2** (c and d) under a 1000 Oe applied DC field.

field (Fig. 3a and b). The data were fit using a Debye model to give an energy barrier of 22.5 K and a pre-exponential factor of $\tau_0 = 3 \times 10^{-7}$ s (Table 1, Fig. S2c†). The measurement was repeated under a 750 Oe applied DC field (Fig. S3†) which results in an energy barrier of 21.2 K and a pre-exponential factor of $\tau_0 = 4.22 \times 10^{-7}$ s. The low frequency field induced χ'' signal was retained in 10% solutions of **1** in 2-MeTHF (Fig. S4–6†) which confirms the molecular origin of the slow relaxation phenomena with an energy barrier of 21.2 K and a pre-exponential factor of $\tau_0 = 1.22 \times 10^{-6}$ s with a second high frequency signal appearing at zero field.

The crystal structure of **2** (Fig. 1b) revealed a pseudo-tetrahedral local coordination environment around the central Co (II) ion which is expected to have the orbitally non-degenerate ground state $^4A_2$ with moderate zero-field splitting (ZFS) parameters as a result of the tetragonal distortions of the crystal field.[36–38] The bond angles around the Co center are slightly distorted from an ideal tetrahedron with Cl–Co–Cl and C–Co–C angles of 103.21(3)° and 124.95(9)°, respectively. The angular distortion parameter $\delta = 2\cdot\mathrm{Td}-(\alpha+\beta)$ where α = L–Co–L and β = X–Co–X angles is an indication of the degree of distortion with the value for **2** being $\delta = -9.16$ which signifies a more flattened geometry than previously reported pseudo-tetrahedral Co(II) complexes (Table 2). The flattened structures are expected to result in negative D values.[36,37]

The χT value of **2** at 300 K is 2.47 emu mol^{-1} K which corresponds to the expected value for one Co(II) ion ($S = 3/2$, $g = 2.3$). Upon decreasing the temperature, the χT value remains constant down to 20 K after which temperature it sharply drops to a minimum of 1.65 emu mol^{-1} K at 2 K (Fig. 2). Both the room temperature χT value and the rapid decrease in the low temperature regime are signatures of appreciable magnetic anisotropy as is the lack of saturation in the magnetization *versus* field data up to 7 T (Fig. S7† inset). The field-dependent magnetization data for **2** at temperatures between 1.8 and 4.5 K (Fig. S7†) are non-superimposable which also supports the presence of significant zero-field splitting. The susceptibility data were fitted using PHI[33] program with $D = -7.7$ cm^{-1}, $E = 1.2$ cm^{-1} and $g = 2.29$. The field-dependent magnetization data were fitted using ANISOFIT2.0[40] resulting in similar values for the zero-field splitting parameters with a $D = -9.02(\pm1)$ cm^{-1}, $E = 1.28(\pm1)$ cm^{-1} and $g = 2.32$ (Fig. 4).

The AC susceptibility measurements for compound **2** revealed a field induced out-of-phase AC signal up to 3 K as

Table 2 Selected examples showing effect of geometric distortion δ on magnetic anisotropy in pseudo-tetrahedral complexes

	δ	D (cm^{-1})	U_{eff} (K)	τ_0	Ref.
CoN_2Cl_2	−1.6	−5.16	—	—	37
CoN_2I_2	+7.48	+9.2	—	—	38
CoP_2Cl_2	−14.1	−11.6	37.1	1.2×10^{-9}	39
CoC_2Cl_2	−9.16	−7.7	20.3	1.7×10^{-8}	**2** [this work]

Table 1 Examples of cobalt complexes with large ZFS parameters in a trigonal planar coordination environment

Compound	μ_{eff}	g	D (cm^{-1})	E (cm^{-1})	U_{eff} (K)	τ_0 (s)
$Co[N(SiMe_2Ph)_2]_2(thf)$[34]	5.2	—	—	—	—	—
$Co[N\text{-}(SiMe_3)_2]_2(thf)$[6,13]	5.883	3.03	−73	14.6	18.1	9.3×10^{-8}
$Co[N(SiMe_3)_2]_2(py)$[13]	5.269	2.722	−82	21	—	—
$Co[N(SiMe_3)_2]_2(PMe_3)$[13]	4.71	2.43	−74	9.6	—	—
$[Na(12\text{-crown-}4)_2][Co\{N(SiMe_3)_2\}_3]$[13]	5.74	2.97	−62	10	—	—
$[Li(15\text{-crown-}5)][Co\{N(SiMe_3)_2\}_3]$[6]	5.25	2.71	−57	12.7	16.1	3.5×10^{-7}
$Co\{N(SiMe_3)_2\}_2(PCy_3)$[6]	5.49	2.84	−82	0	19.1	3×10^{-7}
$[Co\{N(SiMe_3)_2\}_2(SIPr)]$[35]	5.34	2.76	81.6	0	—	—
$[Co\{N(SiMe_3)_2\}_2(SIMes)]$[35]	5.58	2.88	97.2	0	—	—
$[Co\{N(SiMe_3)_2\}_2(PCP)]$[35]	5.46	2.82	113	0	—	—
$[Co\{N(SiMe_3)_2\}_2(PC)]$[35]	5.66	2.92	74.4	0	—	—
$[Co\{N(SiMe_3)_2\}_2(cAACCy)]$[35]	5.34	2.76	114	0	—	—
1 [this work]	5.1	2.63	+73.7	+19.2	22.2	4.2×10^{-7}

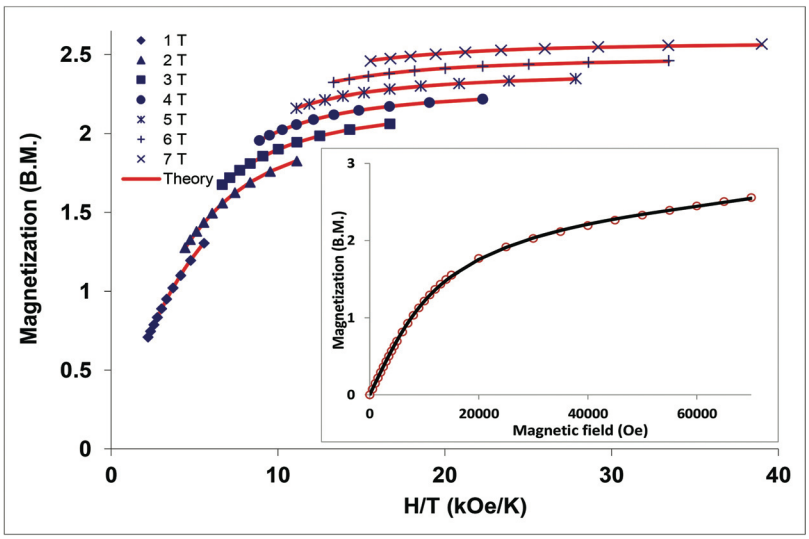

Fig. 4 Reduced magnetization data for **2**. Solid lines correspond to fits using Anisofit2.0 (D = −9.01 cm^{-1}, E = 1.2 cm^{-1}, g = 2.32) inset; field dependent magnetization data at 1.8 K. Solid line corresponds to fit using PHI.

depicted in Fig. 3c and d. The frequency dependent AC measurements of **2** under different applied DC fields revealed an optimum applied DC field of 1000–1500 Oe (Fig. S9a†). The frequency dependent measurements at different temperatures in the range of ν (1–1500 Hz) were measured for the pure sample from 1.8–2.4 K under both 1000 Oe and 1500 Oe DC fields (Fig. S10 and 11†). The data were fit using a Debye model[41] to give an energy barrier of 18.9 K and a pre-exponential factor of $\tau_0 = 2.9 \times 10^{-8}$ s at 1000 Oe and 20.2 K, $\tau_0 = 1.73 \times 10^{-8}$ s at 1500 Oe. The measurement was repeated using a 4% solution in 2-MeTHF (Fig. S9c†) which revealed a slight increase in the position of the χ'' signal albeit with higher noise which renders energy barrier estimates unrealistic.

Compound **3** exhibits a square planar local geometry around the cobalt center with bond angles of almost 90°. Whereas the bond distances are irregular with shorter Co–C_{NHC} (1.915(2) Å) than that of **2**.[20] Such local geometry is expected to lead to a low spin $S = \frac{1}{2}$ magnetic ground state. The χT value of **3** at 300 K (0.46 emu mol^{-1} K, Fig. 2) corresponds to the expected value for one Co(II) ion ($S = \frac{1}{2}$, g = 2.2). As the temperature is lowered, the χT value slowly decreases until ~30 K after which temperature a sharp drop to a minimum of 0.29 emu mol^{-1} K at 2 K is observed (Fig. S12†).

To develop a better understanding of the electronic structure of **1** and **2** and how it relates to the magnetic properties, two step *ab initio* NEVPT2 calculations were performed on both complexes using the ORCA suite.[42] The details are described in the computational section. The resulting energies are listed in Table 3.

The electronic configuration of a Co(II) center in a trigonal planar coordination environment is $(d_{yz}, d_{xz})^4(d_{z^2})^1(d_{x^2-y^2}, d_{xy})^2$. Axial distortions in a C_{2v} symmetry result in a lifting of the orbital degeneracy of the *e*-symmetry orbitals leading to the

Table 3 D, E, g, and energy differences between ground and excited states (ΔE) at the CASSCF and NEVPT2 levels

	1		**2**	
	CASSCF	NEVPT2	CASSCF	NEVPT2
D (cm^{-1})	82.42	75.81	−7.43	−4.54
E/D	0.17	0.17	0.057	0.098
ΔE (cm^{-1})	705.5	1168.3	2861.6	4142.2
g_x	1.8225	1.91325	2.2942	2.2175
g_y	3.0694	2.81807	2.3064	2.2293
g_z	3.2799	3.05799	2.3946	2.2838

$(d_{xy})^2$ $(d_{xz})^2$ $(d_{x^2-y^2})^1$ $(d_{z^2})^1(d_{yz})^1$ configuration.[6] In **1**, the three lower energy states are strongly multi-determinant and non-Aufbau.[43] The dominant electronic configurations for the ground state and the first and second excited states are $(d_{xy})^2(d_{xz})^1(d_{x^2-y^2})^1(d_{z^2})^2(d_{yz})^1$, $(d_{xy})^2(d_{xz})^2(d_{x^2-y^2})^1(d_{z^2})^1(d_{yz})^1$ and $(d_{xy})^2(d_{xz})^1(d_{x^2-y^2})^1(d_{z^2})^1(d_{yz})^2$, respectively (Fig. S13†). The non-degeneracy of the ground state configurations indicates the absence of a first-order spin orbit coupling contribution to the magnetic moment, thus second-order spin orbit coupling *via* mixing with low lying excited states is the only viable explanation for the magnetic anisotropy of the complexes. The major contributions to the positive D value arise from ground to first and ground to second excited states transitions (Table S1†), both of which contribute comparably to the total D value. These excitations occur between orbitals with different m_ℓ values ($\{d_{x^2-y^2}, d_{z^2}\} \rightarrow d_{xz}$) and ($\{d_{z^2}, d_{xy}\} \rightarrow \{d_{x^2-y^2}, d_{yz}\}$) which leads to a positive D value.[44] The positive D value could be also explained in light of the geometric sensitivity towards the dihedral angle between the C–Co–C plane and N–C–N carbene ligand plane which affects metal orbital alignment/mixing with the p-orbital on the carbene ligand.[23] The D

value is inversely proportional to the small excited state splitting leading to a large positive value (+75.8, g_x = 1.91, g_y = 2.81, g_z = 3.05), which is in good agreement with the experimental data (Table 3). The *ab initio* NEVPT2 computed transverse anisotropy parameter, E/D, was found to be 0.17 which leads to appreciable QTM and thus only a field-induced slow paramagnetic relaxation.

In the case of **2**, the dominant ground state electronic configuration is $(d_{z^2})^2\{(d_{xz})(d_{x^2-y^2})\}^3(d_{xy})^1(d_{yz})^1$ similar to the previously reported configuration elucidated using DFT calculations.[45] The multi-determinant first excited state has a dominant configuration of $\{(d_{z^2})(d_{xz})\}^3(d_{x^2-y^2})^1(d_{xy})^2(d_{yz^2})^1$ (Fig. S14†). The major contribution to D arises from $d_{x^2-y^2} \rightarrow d_{xy}$ transitions resulting in negative D value contributions and $d_{xz} \rightarrow d_{xy}$ transitions with smaller positive contributions leading to an overall negative D value of -4.54 cm^{-1} which is expected due to the flattened geometry of the compound. The larger energy separations ($\Delta E_{\mathrm{Root}(1-2/1-3)}$) in **2** leads to much smaller contributions to D.

Conclusions

The present study of the magnetic properties of a series of mononuclear NHC cobalt complexes reveals a large magnetic anisotropy for the trigonal cobalt center (D = +73.3 cm^{-1}) in **1** and a much smaller negative D value (-7.7 cm^{-1}) for **2**. These experimental findings were supported by CASSCF calculations. Despite the different type of anisotropy (easy plane in **1** *vs.* easy axis in **2**), both compounds exhibit slow relaxation of the magnetization below 4 K with an energy barrier (U_{eff}) of 22.5 K for **1** and 18.9 K for **2**. Compound **3** was found to be an $S = \frac{1}{2}$ system. These results add valuable information to the literature of magnetic anisotropy of mononuclear metal complexes and open up new venues for organometallic chemistry in the design of mononuclear SMMs.

Experimental details

All complexes were synthesized following previously reported procedures.[20] Each compound was isolated and its composition verified by ^{1}H NMR spectroscopy. Single crystals of each compound were then grown to ensure high purity prior magnetic measurements (see details in ESI†). DC magnetic susceptibility measurements were performed on crushed single crystals of the compounds with the use of a Quantum Design MPMS-XL SQUID magnetometer operating in the temperature range of 1.8–300 K at 1000 G. The diamagnetic contribution of the polypropylene bag was subtracted from the raw data. Pascal's constants[1] were used to estimate the diamagnetic corrections of the atoms, which were subtracted from the experimental susceptibilities to give the molar paramagnetic susceptibilities (χ_{M}). AC magnetic susceptibility measurements were performed on the same sample with an oscillating field of 3 Oe in the range of 1–1500 Hz.

Computational details

Single point calculations were performed using the crystallographic geometries provided in the cif files. The two-step approach implemented in the ORCA 4.1.0 program with the spin–orbit coupling (SOC) and spin–spin coupling (SSC) relativistic effects included was used to conduct *ab initio* calculations.[2] Several solutions of the non-relativistic Born–Oppenheimer Hamiltonian were calculated using a complete active space self-consistent field (CASSCF) in the first step. The electronic configuration of Co(II) is d^7, so the selected active space CAS(7,5) contains 7 electrons in the 5 essentially atomic d orbitals.[3] Secondly, the effect of SOC and SSC were taken into account using the quasi-degenerate perturbation theory (QDPT). N-Electron Valence Perturbation Theory (NEVPT2) was employed to evaluate the effects of the dynamic correlations by substituting the diagonal elements of the QDPT matrix with the NEVPT2 corrected state energies. The auxiliary def2-TZV/C basis set for resolution of identity (RI) approximation and the Karlsruhe polarized triple-z basis set (TZVP), were employed.[4]

Conflicts of interest

There are no conflicts to declare.

Acknowledgements

KRD thanks the National Science Foundation (NSF CHE-1808779) and the Welch Foundation (A-1449) for financial support. We also thank the HPRC at Texas A&M University for the computing resources. ZJT thanks the Welch Foundation (AX-1772).

Notes and references

1 J. J. Le Roy, M. Jeletic, S. I. Gorelsky, I. Korobkov, L. Ungur, L. F. Chibotaru and M. Murugesu, *J. Am. Chem. Soc.*, 2013, **135**, 3502–3510.
2 M. R. Saber and K. R. Dunbar, *Chem. Commun.*, 2014, **50**, 2177–2179.
3 J. M. Zadrozny, D. J. Xiao, M. Atanasov, G. J. Long, F. Grandjean, F. Neese and J. R. Long, *Nat. Chem.*, 2013, **5**, 577–581.
4 A. J. Brown, D. Pinkowicz, M. R. Saber and K. R. Dunbar, *Angew. Chem., Int. Ed.*, 2015, **54**, 5864–5868.
5 J. M. Zadrozny and J. R. Long, *J. Am. Chem. Soc.*, 2011, **133**, 20732–20734.
6 A. Eichhöfer, Y. Lan, V. Mereacre, T. Bodenstein and F. Weigend, *Inorg. Chem.*, 2014, **53**, 1962–1974.
7 D. Weismann, Y. Sun, Y. Lan, G. Wolmershäuser, A. K. Powell and H. Sitzmann, *Chem. – Eur. J.*, 2011, **17**, 4700–4704.
8 S. Gomez-Coca, E. Cremades, N. Aliaga-Alcalde and E. Ruiz, *J. Am. Chem. Soc.*, 2013, **135**, 7010–7018.

9 J. Vallejo, I. Castro, R. Ruiz-Garcia, J. Cano, M. Julve, F. Lloret, G. De Munno, W. Wernsdorfer and E. Pardo, *J. Am. Chem. Soc.*, 2012, **134**, 15704–15707.
10 Y.-Z. Zhang, S. Gomez-Coca, A. J. Brown, M. R. Saber, X. Zhang and K. R. Dunbar, *Chem. Sci.*, 2016, **7**(10), 6519–6527.
11 A. Buchholz, A. O. Eseola and W. Plass, *C. R. Chim.*, 2012, **15**, 929–936.
12 T. Jurca, A. Farghal, P.-H. Lin, I. Korobkov, M. Murugesu and D. S. Richeson, *J. Am. Chem. Soc.*, 2011, **133**, 15814–15817.
13 A. M. Bryan, G. J. Long, F. Grandjean and P. P. Power, *Inorg. Chem.*, 2013, **52**, 12152–12160.
14 Y. Y. Zhu, C. Cui, Y. Q. Zhang, J. H. Jia, X. Guo, C. Gao, K. Qian, S. D. Jiang, B. W. Wang, Z. M. Wang and S. Gao, *Chem. Sci.*, 2013, **4**, 1802–1806.
15 M. R. Saber, M. K. Singh and K. R. Dunbar, *Chem. Commun.*, 2020, **56**, 8492–8495.
16 S. A. Sulway, R. A. Layfield, F. Tuna, W. Wernsdorfer and R. E. P. Winpenny, *Chem. Commun.*, 2012, **48**, 1508–1510.
17 S.-D. Jiang, S.-S. Liu, L.-N. Zhou, B.-W. Wang, Z.-M. Wang and S. Gao, *Inorg. Chem.*, 2012, **51**, 3079–3087.
18 S.-D. Jiang, B.-W. Wang, H.-L. Sun, Z.-M. Wang and S. Gao, *J. Am. Chem. Soc.*, 2011, **133**, 4730–4733.
19 M. Jeletic, P. H. Lin, J. J. Le Roy, I. Korobkov, S. I. Gorelsky and M. Murugesu, *J. Am. Chem. Soc.*, 2011, **133**, 19286–19289.
20 J. A. Przyojski, H. D. Arman and Z. J. Tonzetich, *Organometallics*, 2013, **32**, 723–732.
21 F.-S. Guo, A. K. Bar and R. A. Layfield, *Chem. Rev.*, 2019, **119**, 8479–8505.
22 A. A. Danopoulos, P. Braunstein, M. Wesolek, K. Y. Monakhov, P. Rabu and V. Robert, *Organometallics*, 2012, **31**, 4102–4105.
23 J. J. Dunsford, D. J. Evans, T. Pugh, S. N. Shah, N. F. Chilton and M. J. Ingleson, *Organometallics*, 2016, **35**, 1098–1106.
24 P. H. Lin, N. C. Smythe, S. I. Gorelsky, S. Maguire, N. J. Henson, I. Korobkov, B. L. Scott, J. C. Gordon, R. T. Baker and M. Murugesu, *J. Am. Chem. Soc.*, 2011, **133**, 15806–15809.
25 M. Damjanović, P. P. Samuel, H. W. Roesky and M. Enders, *Dalton Trans.*, 2017, **46**, 5159–5169.
26 R. C. Poulten, M. J. Page, A. G. Algarra, J. J. Le Roy, I. Lopez, E. Carter, A. Llobet, S. A. Macgregor, M. F. Mahon, D. M. Murphy, M. Murugesu and M. K. Whittlesey, *J. Am. Chem. Soc.*, 2013, **135**, 13640–13643.
27 Y.-S. Meng, Z. Mo, B.-W. Wang, Y.-Q. Zhang, L. Deng and S. Gao, *Chem. Sci.*, 2015, **6**, 7156–7162.
28 P. L. Holland, T. R. Cundari, L. L. Perez, N. A. Eckert and R. J. Lachicotte, *J. Am. Chem. Soc.*, 2002, **124**, 14416–14424.
29 H. Andres, E. L. Bominaar, J. M. Smith, N. A. Eckert, P. L. Holland and E. Münck, *J. Am. Chem. Soc.*, 2002, **124**, 3012–3025.
30 T. R. Dugan, J. M. Goldberg, W. W. Brennessel and P. L. Holland, *Organometallics*, 2012, **31**, 1349–1360.
31 K. L. Fillman, J. A. Przyojski, M. H. Al-Afyouni, Z. J. Tonzetich and M. L. Neidig, *Chem. Sci.*, 2015, **6**, 1178–1188.
32 S. A. Stoian, Y. Yu, J. M. Smith, P. L. Holland, E. L. Bominaar and E. Münck, *Inorg. Chem.*, 2005, **44**, 4915–4922.
33 N. F. Chilton, R. P. Anderson, L. D. Turner, A. Soncini and K. S. Murray, *J. Comput. Chem.*, 2013, **34**, 1164–1175.
34 S. N. König, C. Schädle, C. Maichle-Mössmer and R. Anwander, *Inorg. Chem.*, 2014, **53**, 4585–4597.
35 A. Massard, P. Braunstein, A. A. Danopoulos, S. Choua and P. Rabu, *Organometallics*, 2015, **34**(11), 2429–2438.
36 M. Idešicová, J. Titiš, J. Krzystek and R. Boča, *Inorg. Chem.*, 2013, **52**, 9409–9417.
37 J. Titiš, J. Miklovič and R. Boča, *Inorg. Chem. Commun.*, 2013, **35**, 72–75.
38 M. R. Saber and K. R. Dunbar, *Chem. Commun.*, 2014, **50**, 12266–12269.
39 F. Yang, Q. Zhou, Y. Zhang, G. Zeng, G. Li, Z. Shi, B. Wang and S. Feng, *Chem. Commun.*, 2013, **49**, 5289–5291.
40 M. P. Shores, J. J. Sokol and J. R. Long, *J. Am. Chem. Soc.*, 2002, **124**, 2279–2292.
41 K. S. Cole and R. H. Cole, *J. Chem. Phys.*, 1941, **9**, 341–351.
42 F. Neese, *WIREs Comput. Mol. Sci.*, 2018, **8**, e1327.
43 P. C. Bunting, M. Atanasov, E. Damgaard-Møller, M. Perfetti, I. Crassee, M. Orlita, J. Overgaard, J. van Slageren, F. Neese and J. R. Long, *Science*, 2018, **362**(6421), eaat7319.
44 M. K. Singh, P. Shukla, M. Khatua and G. Rajaraman, *Chem. – Eur. J.*, 2020, **26**, 464–477.
45 T. E. Iannuzzi, Y. Gao, T. M. Baker, L. Deng and M. L. Neidig, *Dalton Trans.*, 2017, **46**, 13290–13299.